Asian Journal of Control, Vol. 20, No. 4, pp. 1352–1366, July 2018
Published online 12 December 2016 in Wiley Online Library (wileyonlinelibrary.com) DOI: 10.1002/asjc.1422

A COMPARISON OF SCANNING METHODS AND THE VERTICAL CONTROL IMPLICATIONS FOR SCANNING PROBE MICROSCOPY

Yik R. Teo, Yuen Yong, and Andrew J. Fleming

ABSTRACT

This article compares the imaging performance of non-traditional scanning patterns for scanning probe microscopy including sinusoidal raster, spiral, and Lissajous patterns. The metrics under consideration include the probe velocity, scanning frequency, and required sampling rate. The probe velocity is investigated in detail as this quantity is proportional to the required bandwidth of the vertical feedback loop and has a major impact on image quality. By considering a sample with an impulsive Fourier transform, the effect of scanning trajectories on imaging quality can be observed and quantified. The non-linear trajectories are found to spread the topography signal bandwidth which has important implications for both low and high-speed imaging. These effects are studied analytically and demonstrated experimentally with a periodic calibration grating.

Key Words: Scanning probe microscopy, scanning methods.

I. INTRODUCTION

Scanning probe microscopy (SPM) is a family of imaging methods that operate by scanning a sample with a physical probe [1]. The most popular forms of SPM are the Scanning Tunnelling Microscope(STM) [2] and the Atomic Force Microscope (AFM) [3]. In an SPM, the sample is typically mounted on a two-axis positioner that moves in the lateral directions. The interactions between the probe and sample in the vertical direction are recorded and used to construct the image. The foremost factors limiting the image quality, resolution and speed of SPMs are the bandwidth of the lateral scanner and the closed-loop bandwidth of the vertical feedback system.

The bandwidth limitations of the lateral scanner are mainly due to the mechanical dynamics [4]. However, in recent years, a considerable improvement in the speed of SPMs has been achieved with the use of advanced control techniques, for example, feed-forward control [5], improved feedback control [6–10] and methods such as input shaping [11,12]

Further improvements in scanning speed have been achieved through the introduction of novel scanning trajectories. The traditional scanning method in SPMs is raster scanning, which involves driving the x-axis (fast axis) with a triangular trajectory and shifting the sample in steps or continuously in the y-axis (slow axis). Due to the low bandwidth and potentially resonant nature of the positioning stage, the harmonics may result in significant tracking error and undesirable vibration. Consequentially, the frequency of triangular raster scanning is typically limited to 1–10% of the first resonance frequency of the positioner [13]. The triangular signal bandwidth can be reduced by smoothing the trajectory [11] but at the expense of linear scanning range. The primary advantages of raster scanning are the constant velocity and simple image reconstruction which is due to regularly sampled data appearing on a square grid.

Alternative scanning methods based on sinusoidal trajectories include sinusoidal raster, spiral, Lissajous and cycloid methods. Sinusoidal raster scanning involves driving the x-axis (fast axis) with a sinusoidal trajectory while shifting the sample in steps or continuously in the y-axis (slow axis) [14–16]. Spiral, Lissajous and cycloid scanning methods require sinusoidal trajectories in both the x and y axes. Spiral scanning was first proposed in [17] and has been well studied in the literature [18–23]. Similarly, the application of Lissajous scanning pattern in SPM can be found in [24–26]. The cycloid scan pattern involves a sinusoidal trajectory in one axis and a sinusoidal trajectory plus a ramp input in the other axis [27]. The major benefit of a sinusoidal trajectory is the single-tone frequency spectrum. As a result, the scan rate can be close to, or above, the first resonance frequency of the positioner. However, the drawbacks include non-uniform spatial sampling, a sinusoidal veloc-

Manuscript received 5 April 2016; revised 23 June 2016; accepted 28 August 2016.

All authors are with the Precision Mechatronics Lab at the School of Electrical Engineering and Computer Science, The University of Newcastle, 2308 Callaghan, New South Wales, Australia (e-mail: [yik.teo, yuenkuan.yong, andrew.fleming]@newcastle.edu.au)

Yik Teo is the corresponding author (e-mail: yik.teo@newcastle.edu.au)

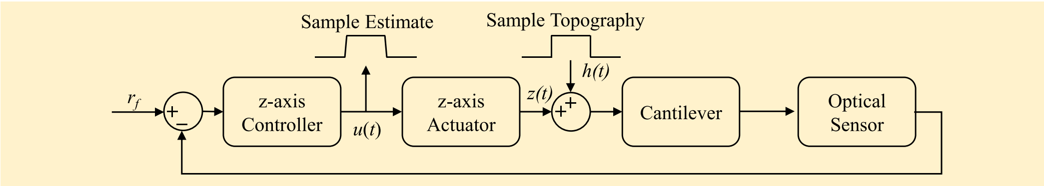

(a) Vertical feedback control system for constant-force contact-mode where r_f is the force reference.

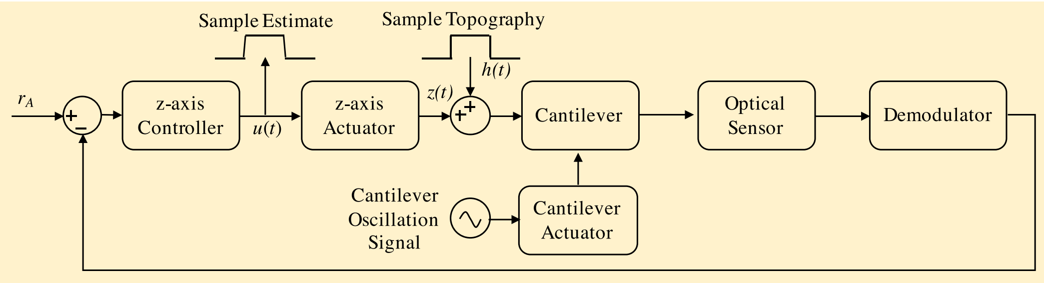

(b) Vertical feedback control system for tapping-mode where r_A is the cantilever oscillation amplitude reference.

Fig. 1. Typical vertical feedback control systems for constant-force contact-mode (a) and constant-amplitude tapping-mode (b). The sample topography $h(t)$ acts as an input disturbance on the feedback loop. When the tracking error is small, the control signal $u(t)$ estimates the sample topography $h(t)$ since $u(t)$ is proportional to height. [Color figure can be viewed at wileyonlinelibrary.com]

ity profile, and the need for interpolation on to a normal grid using methods such as the Delaunay triangulation technique [28,29].

The imaging modes of scanning probe microscopes can be grouped by the type of contact that occurs, either constant contact, non-contact, or intermittent contact modes. Examples of constant contact modes include constant-force contact-mode and constant-height contact-mode. A typical vertical feedback loop for constant-force contact-mode is shown in Fig. 1a. An example of a control loop for constant-amplitude intermittent contact mode (tapping mode) [30], is shown in Fig. 1b. All imaging modes require a vertical feedback controller except constant height modes, which do not regulate the contact force and are therefore rarely used.

The bandwidth of the vertical feedback loop is crucial as the sample topography appears as a disturbance $h(t)$ which must be regulated. The vertical bandwidth can be increased by modifying the hardware, for example, by implementing a dual-stage scanner in the vertical axis [31] or by increasing the scanner resonance frequency [6,32]. An alternative method for improving imaging quality is to reduce the bandwidth of the topography signal $h(t)$, for example, by using a saw-tooth trajectory which reduces the velocity.

Contribution of this work. The contribution of this work is to investigate the relationship between the lateral scanning method and the bandwidth of the topography signal $h(t)$. In Section II, the popular scanning methods in the literature are compared in a uniform framework. In Section III, the relationships between the scan rate, imaging time, resolution and sampling frequency are discussed. Then in Section IV, the lateral control implications of each scanning method are discussed qualitatively. In Section V, the probe velocity of each scanning method is compared. Finally, the relationship between the image quality and vertical feedback bandwidth is described in Section VI.

II. SCANNING METHODS

In this section, the methods under consideration are described including: raster, sinusoidal raster, spiral and Lissajous scanning method. Analytical expressions for the scan rate, imaging time and sampling frequency are derived and compared. As an example, a $5 \times 5\mu$m scan with 1 μm resolution is considered so that the individual sampling points can be clearly observed. All of the scanning methods have a fixed imaging time of 3.6 s.

2.1 Raster scan

A traditional raster scan involves a triangular trajectory in the x-axis while shifting the sample position in steps or continuously in the y-axis. The resolution is the ratio of scan size and pixels per line (N). For a square image, the resolution in the x- and y-axis is

$$x_{\text{res}} = y_{\text{res}} = \frac{x_{\text{size}}}{N}.$$

where x_{size} is the image width. The raster period T_{raster} and scanning frequency f_{raster} is

$$T_{\text{raster}} = \frac{2(N-1)}{f_s} \qquad f_{\text{raster}} = \frac{1}{T_{\text{raster}}},$$

where f_s is the sampling frequency. The total imaging time T_{end} is

$$T_{\text{end}} = \frac{N-0.5}{f_{\text{raster}}}. \tag{1}$$

There are multiple methods for driving the y-axis (slow-axis), including a ramp, stairs and smooth stairs. The image and scan trajectories for each method are plotted in Fig. 2. The image is a $5 \times 5\mu m$ scan with a $1\mu m$ resolution and a fixed imaging time of 3.6 s. This requires a 1.25-Hz scan rate and 10-Hz sampling frequency.

In this work, the ramp method is considered as this is most suited to high speed imaging. The resulting image in Fig. 3a is a parallelogram with sides of equal length

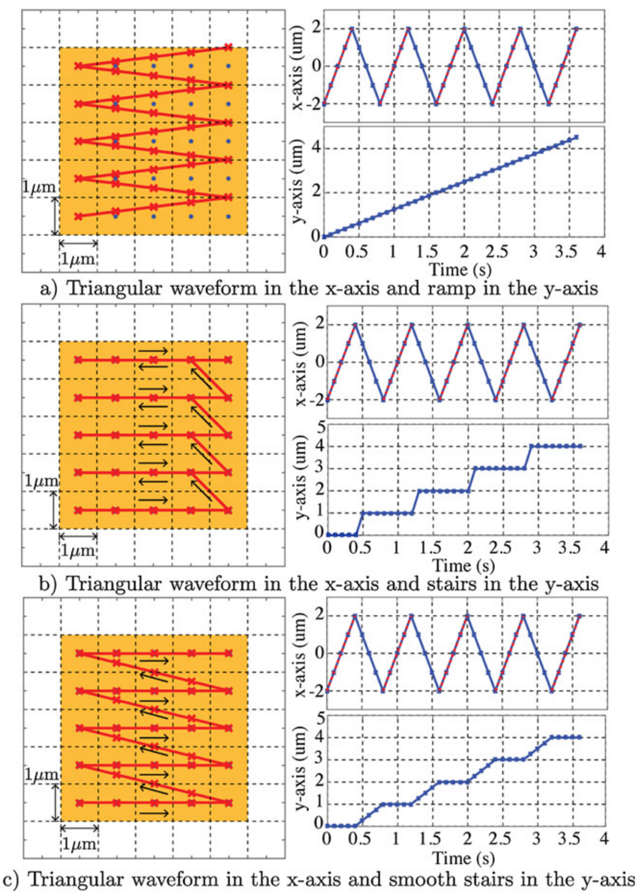

Fig. 2. A comparison of different raster scan methods in the y-axis. [Color figure can be viewed at wileyonlinelibrary.com]

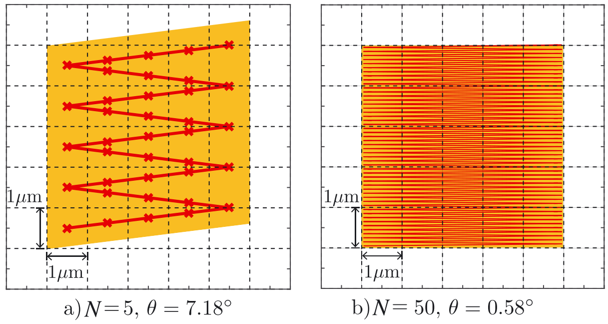

Fig. 3. Reconstructed image (rhombus). [Color figure can be viewed at wileyonlinelibrary.com]

(equilateral), also known as a rhombus. The small skew angle is often considered to be negligible, which is

$$\theta = \arcsin\left(\frac{0.5}{N-1}\right).$$

An advantage of driving the y-axis with a stair or smooth stair waveform is the precisely square image; however, these waveforms may complicate the control design in high-speed applications due to the required step changes.

2.2 Sinusoidal raster scan

In sinusoidal raster scanning, the triangular trajectory is replaced by a sinusoidal trajectory in the x-axis (fast axis) and the sample is shifted in steps or continuously in the y-axis (slow axis). The different sinusoidal raster methods are plotted in Fig. 4. Here, the ramp waveform is considered.

Due to the non-uniform sampling distance of a sinusoidal waveform, the resolution is defined as the furthest distance between two adjacent points,

$$x_{\text{res}} = \frac{(x_{\text{size}} - x_{\text{size}}/N)}{2} \sin\left(\frac{2\pi f_{\sin}}{f_s}\right),$$

where N is the number of pixels per line and $f_{\sin}$ is the scanning frequency. If the desired resolution and scanning frequency is fixed, the minimum sampling frequency is

$$f_s = 2\pi f_{\sin}\left[\arcsin\left(\frac{2}{N-1}\right)\right]^{-1}. \tag{2}$$

The imaging time for a sinusoidal raster scan is

$$T_{\text{end}} = \frac{(N-0.5)}{f_{\sin}}. \tag{3}$$

Fig. 4a shows a $5 \times 5\mu m$ scan with a fixed imaging time of 3.6 s and a resolution of $1\mu m$. This requires a scanning frequency of 1.25 Hz and a sampling rate of 15 Hz.

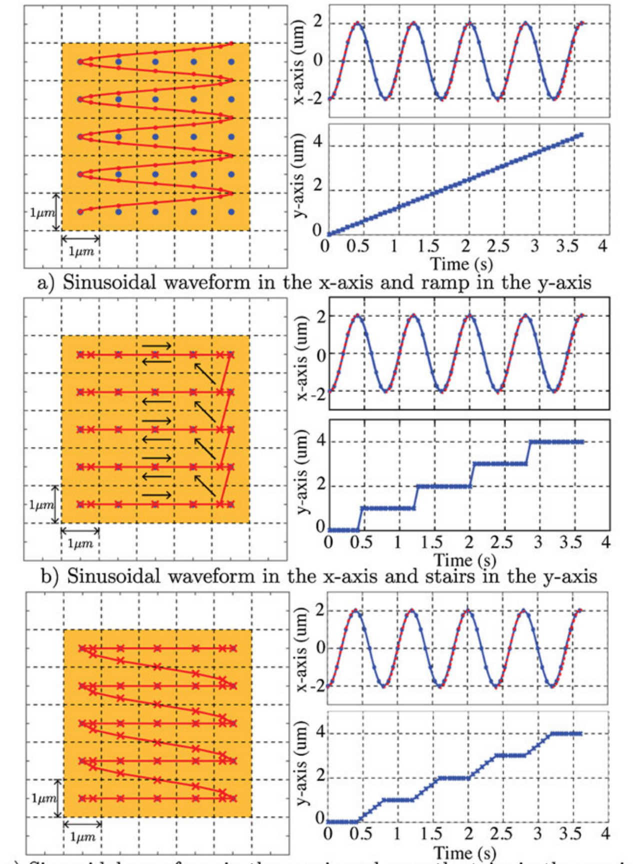

a) Sinusoidal waveform in the x-axis and ramp in the y-axis

b) Sinusoidal waveform in the x-axis and stairs in the y-axis

c) Sinusoidal waveform in the x-axis and smooth stairs in the y-axis

Fig. 4. A comparison of different sinusoidal raster scan methods in the y-axis. [Color figure can be viewed at wileyonlinelibrary.com]

2.3 Spiral scan

The x and y trajectories of a spiral scan consist of a sinusoidal and cosine reference of the same frequency but varying amplitude. The trajectories are

$$x(t) = r(t)\cos(2\pi f_{\mathrm{spiral}} t),$$
$$y(t) = r(t)\sin(2\pi f_{\mathrm{spiral}} t).$$

where f_{spiral} is the scanning frequency and the radius $r(t)$ varies with time.

In this work, the constant angular velocity method (CAV) is considered as this has the advantage of a constant frequency [22]. The equation that generates a CAV spiral of pitch P at an angular velocity of ω is derived from the differential equation

$$\frac{\mathrm{d}r}{\mathrm{d}t} = \frac{P\omega}{2\pi},$$

where r is the instantaneous radius at time t. The solution of the equationabove with $r = 0$ and $t = 0$ is

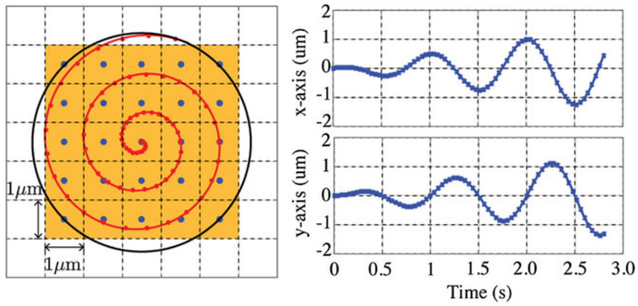

Fig. 5. Spiral scan of a 5 μm image with constant angular velocity. [Color figure can be viewed at wileyonlinelibrary.com]

$$r(t) = \frac{P}{2\pi}\omega t,$$

where the pitch P is

$$P = \frac{\text{spiral radius} \times 2}{\text{number of curves} - 1}.$$

The number of curves is the number of times the spiral curve crosses through the line $y = 0$. The pitch distance P defines the resolution. The imaging time is

$$T_{\mathrm{end}} = \frac{2\pi r_{\mathrm{end}}}{P\omega},$$

where r_{end} is the largest radius of the spiral.

An advantage of this method is that it involves tracking a single frequency sinusoid with a slowly varying amplitude. The image and scan trajectory of a spiral scan is illustrated in Fig. 5.

2.4 Lissajous scan

The Lissajous trajectory is achieved by driving the x and y axes with purely sinusoidal signals of different frequency, that is,

$$x(t) = A_x\cos(2\pi f_x t),$$
$$y(t) = A_y\cos(2\pi f_y t).$$

The shape of the Lissajous pattern is dependent on the ratio f_x/f_y and the phase difference between the two sinusoids. If the phase difference between the x and y signals is zero, the frequency difference between f_x and f_y determines the period T in which the pattern evolves and repeats itself. T is defined as

$$T = \frac{1}{|f_x - f_y|}.$$

The ratio of x and y frequencies should be a rational number [24],

$$\frac{f_x}{f_y} = \frac{2M}{2M-1}, \tag{4}$$

where M is a positive integer. The path traversed during the first half period is symmetric with respect to the x-axis, hence, a square-shaped region can be fully scanned using a half-period Lissajous pattern.

The resolution of a Lissajous scanning pattern is considered to be the maximum distance between scan lines. The lowest resolution generally occurs in the center of the image, which is approximately [24],

$$l_{\text{res}} \approx \frac{\pi A_x A_y}{M\sqrt{A_x^2 + A_y^2}}.$$

The minimum imaging time is

$$T_{\text{end}} = \frac{M}{f_x} \approx \frac{\pi A_x A_y}{f_x l_{\text{res}}\sqrt{A_x^2 + A_y^2}},$$

and the minimum sampling frequency is

$$f_s = 2(2M-1)f_x.$$

If the desired resolution l_{res} is 1 μm, M is

$$M = \left\lceil \frac{\pi A_x A_y}{l_{\text{res}}\sqrt{A_x^2 + A_y^2}} \right\rceil = 5,$$

where the half brackets represent the ceiling function and $A_x = A_y = (x_{\text{size}} - x_{\text{res}})/2$. The scanning frequencies are

$$f_x = \frac{M}{T_{\text{end}}},$$
$$f_y = \frac{2M-1}{2M} f_x.$$

For a 5μm scan with a 1μm resolution and a fixed imaging time of 3.6 s, the scan rates are $f_x = 1.39$ Hz and $f_y = 1.25$ Hz and the minimum sampling frequency is $f_s = 25$ Hz. The scan trajectory of the Lissajous method is plotted in Fig. 6.

III. SCANNING FREQUENCY, IMAGING TIME, RESOLUTION AND SAMPLING FREQUENCY

In this section, the required scanning and sampling frequency are related to the desired imaging time and resolution.

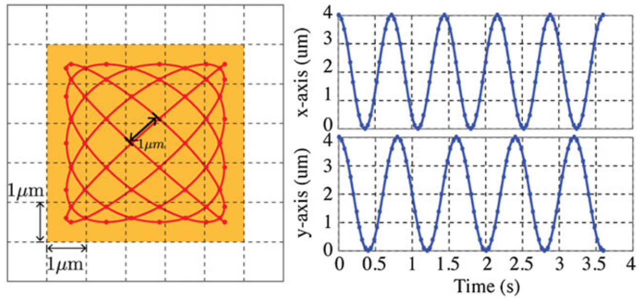

Fig. 6. Lissajous scan of a 5μm image. [Color figure can be viewed at wileyonlinelibrary.com]

For a raster scan, the relationship between the scanning frequency and resolution is

$$f_{\text{raster}} = \frac{N-0.5}{T_{\text{end}}} \approx \frac{N}{T_{\text{end}}}.$$

The relationship between the sampling frequency and resolution is

$$f_s = 2(N-1)f_{\text{raster}} = \frac{2(N-1)(N-0.5)}{T_{\text{end}}}.$$

For a sinusoidal raster scan, the relationship between the scanning frequency and imaging time is identical to the raster scan, that is

$$f_{\sin} = \frac{N-0.5}{T_{\text{end}}} \approx \frac{N}{T_{\text{end}}}. \tag{5}$$

For a fixed imaging time, the scanning frequency for sinusoidal raster is similar to raster scanning. The relationship between the sampling frequency and resolution is

$$f_s = 2\pi f_{\sin}\left[\arcsin\left(\frac{2}{N-1}\right)\right]^{-1}.$$

For spiral scan, the radius r_{end} should encompass the square image.

$$r_{\text{end}} = \sqrt{x_{\text{size}}^2 + x_{\text{size}}^2} = \sqrt{2}x_{\text{size}} \tag{6}$$

The relationship between the scanning frequency and the resolution is

$$f_{\text{spiral}} = \frac{N}{\sqrt{2}T_{\text{end}}} \approx 0.7071 f_{\text{raster}}$$

This expression shows that the scanning frequency for a spiral scan is approximately 30% slower than the conventional raster scanning and sinusoidal raster scanning methods. The minimum sampling frequency and resolution is [27],

$$f_s = 4Nf_{\text{spiral}} = \frac{4N^2}{\sqrt{2}T_{\text{end}}}.$$

Table I. Analytical expressions for the required scan rate and sampling frequency for a given imaging time and resolution.

Scanning Method	Scanning Frequency	Sampling Frequency
Raster	$\frac{N}{T_{\text{end}}}$	$\frac{2(N-1)(N-0.5)}{T_{\text{end}}}$
Sinusoidal Raster	$\frac{N}{T_{\text{end}}}$	$\frac{2\pi N}{T_{\text{end}}}\left(\arcsin\left(\frac{2}{N-1}\right)\right)^{-1}$
Lissajous	$\lceil\frac{N\pi}{2\sqrt{2}}\rceil\frac{1}{T_{\text{end}}}$	$\left(2\lceil\frac{N\pi}{2\sqrt{2}}\lceil-1\right)\lceil\frac{N\pi}{2\sqrt{2}}\rceil\frac{2}{T_{\text{end}}}$
Spiral	$\frac{N}{\sqrt{2}T_{\text{end}}}$	$\frac{4N^2}{\sqrt{2}T_{\text{end}}}$

Table II. A comparison of scanning frequencies and sampling frequencies for a 10μm scan with an imaging time of 1 s and 128 pixels-per-line.

Scan Method	Scanning Frequency	Sampling Frequency
Raster	127.5 Hz	32.38 kHz
Sinusoidal Raster	127.5 Hz	50.87 kHz
Lissajous	142.0 Hz	80.37 kHz
Spiral	90.1 Hz	46.34 kHz

Table III. Characteristics of Lateral Scanning Trajectories.

Parameter	Raster Scan	Sinusoidal Scan	Spiral Scan	Lissajous Scan
Scan Rate	f_{raster}	f_{raster}	$0.707f_{\text{raster}}$	$1.1f_{\text{raster}}$
Signal Bandwidth	$10f_{\text{raster}}$	f_{raster}	$0.707f_{\text{raster}}$	$1.1f_{\text{raster}}$
Suitable for scan near/above resonance	No	Yes	Yes	Yes
Square Image	Yes	Yes	No	Yes
Repetitive Reference	Yes	Yes	No	Yes
Suitable for simple Internal Model Control	No	Yes	Yes	Yes
Suitable for Repetitive Control	Yes	Yes	No	Yes

For Lissajous scan, the relationship between the scanning frequency and resolution is

$$f_x = \frac{M}{T_{\text{end}}}, \tag{7}$$

where M is given by

$$M = \lceil\frac{\pi A_x A_y}{l_{\text{res}}\sqrt{A_x^2 + A_y^2}}\rceil = \lceil\frac{N\pi}{2\sqrt{2}}\rceil.$$

where $A_x = A_y = A \approx x_{\text{size}}/2$. For a Lissajous scan, the scanning frequency in the x-axis f_x is always greater than the scanning frequency in the y-axis f_y, see (4). Hence, the relationship between minimum sampling frequency and resolution is

$$f_s = 2(2M-1)f_x = \left(2\lceil\frac{N\pi}{2\sqrt{2}}\rceil - 1\right)\lceil\frac{N\pi}{2\sqrt{2}}\rceil\frac{2}{T_{\text{end}}}.$$

To compare the required scanning frequency of the Lissajous method to raster scanning, the imaging times can be equated by substituting (3) into (7), resulting in

$$f_x = \frac{f_{\sin}}{N-0.5}M, \tag{8}$$

where M can be written as

$$M = \lceil\frac{N\pi}{2\sqrt{2}}\rceil \geq \frac{N\pi}{2\sqrt{2}}.$$

This simplifies (8) to

$$f_x = \frac{f_{\sin}}{N-0.5}\lceil\frac{N\pi}{2\sqrt{2}}\rceil. \tag{9}$$

If $N \gg 0.5$, Equation (9) simplifies to

$$\frac{f_x}{f_{\sin}} \approx \frac{\pi}{2\sqrt{2}}. \tag{10}$$

This expression shows that the scanning frequency for a Lissajous scan must be at least 11% higher than the conventional raster scanning and sinusoidal raster scanning methods.

Table I summarizes the required scanning and sampling frequency for each method. As an example, a 10μm scan is considered with an imaging time of 1 s and 128 pixels-per-line. The required scanning frequencies and sampling frequencies of each method are listed in Table II. The raster and sinusoidal raster scans have a scanning frequency of 127.5 Hz but the Lissajous scan is 11 % faster and the spiral scan is 30% slower. In addition, raster scanning requires the lowest sampling frequency followed by spiral scan, sinusoidal raster and Lissajous scans.

IV. LATERAL CONTROL IMPLICATIONS

The lateral scanning system is typically controlled by the combination of feed-forward control [5] and feedback control [6–8]. Due to the low resonance frequency of the scanner, typically in the hundreds of hertz, the bandwidth is limited to the first resonance frequency of the system. In Table III, a summary of the scanning methods and their associated control implications are compared qualitatively.

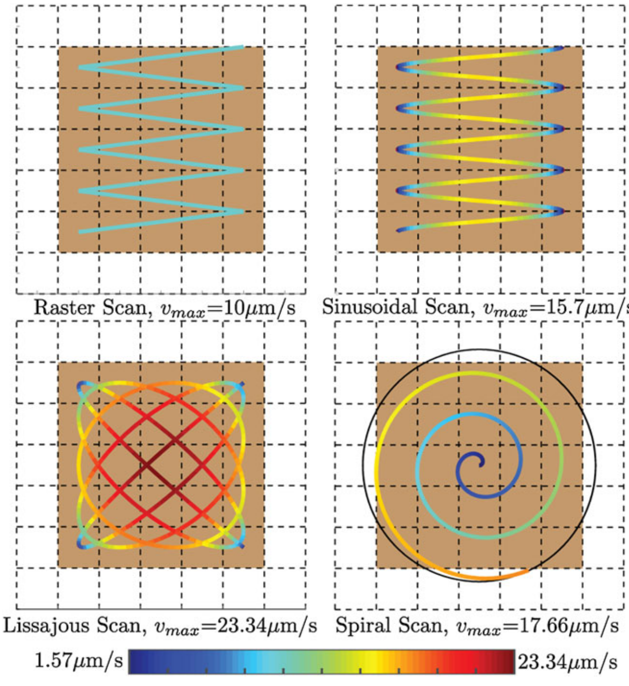

Fig. 7. A comparison of the velocity for a $5 \times 5\mu$m scan with 1μm resolution and an imaging time of 3.6 s. [Color figure can be viewed at wileyonlinelibrary.com]

In spiral scanning, the frequency of the modulating amplitude is much lower than the frequency of the sinusoidal reference. Therefore, the reference signal bandwidth is approximately the frequency of the sinusoidal reference, which is also the lowest frequency of the methods considered. The sinusoidal raster and Lissajous methods provide the next lowest reference signal bandwidth due to the tonal spectra. In comparison, the reference signal bandwidth of a triangular raster trajectory is approximately 10 times the scanning frequency when the first five harmonics are considered.

There are a number of cases where the nature of the scan trajectory can be exploited. For instance, periodic reference signals allow the use of methods such as Repetitive Control [33]. Repetitive control has proven to be effective in tracking triangular waveforms [34–38]. For sinusoidal trajectories, Internal Model Control (IMC) has a low complexity and provides excellent tracking performance for sinusoidal raster scanning, Lissajous scanning [24,26], and spiral scanning [39–41].

V. PROBE VELOCITY

The probe velocity has a significant impact on the imaging quality since many of the interaction forces are a function of velocity, for example, lateral forces and friction. These forces are preferably kept constant during a scan. The probe velocity also impacts the bandwidth of the topography $h(t)$ which appears as a disturbance in the vertical feedback loop, see Fig. 1a. To minimize imaging artefacts, the topography $h(t)$ must be within the bandwidth of the vertical feedback system. Therefore, it is important to understand the relationship between the lateral scanning velocity and vertical bandwidth. The maximum frequency in the topography signal $f_h^{\max}$ is

$$f_h^{\max} \approx \frac{v_{\max}}{T_{\text{profile}}} \text{ Hz}$$

where $v_{\max}$ is the maximum velocity (μm/s) and T_{profile} is the period of the profile (μm/period). The reciprocal of the period of the profile is f_{profile}

$$f_{\text{profile}} = \frac{1}{T_{\text{profile}}} (\text{period}/\mu\text{m}).$$

Table IV summarizes the analytical velocity expressions for each scanning method. As an example, the linear velocity for a $5 \times 5\mu$m scan with parameters in Section II is plotted in Fig. 7. This figure illustrates the varying probe velocity associated with sinusoidal scanning methods.

Table IV. Analytical expressions for the linear and maximum velocity.

Scanning Method	Linear Velocity	Maximum Velocity
Raster	$v(t) = 2(x_{\text{size}} - x_{\text{res}})f_{\text{raster}}$	$v_{\max} = 2(x_{\text{size}} - x_{\text{res}})f_{\text{raster}}$
Sinusoidal Raster	$v(t) = \pi(x_{\text{size}} - x_{\text{res}})f_{\sin}\cos(2\pi f_{\sin} t)$	$v_{\max} = \left[(x_{\text{size}} - x_{\text{res}})\pi\right] f_{\sin}$
Spiral	$v(t) = \sqrt{v_x(t)^2 + v_y(t)^2}$, where $\gamma = P\omega/2\pi$ $v_x(t) = \gamma\cos(2\pi f_{\text{spiral}} t) - 2\pi f_{\text{spiral}}\gamma t\sin(2\pi f_{\text{spiral}} t)$, $v_y(t) = \gamma\sin(2\pi f_{\text{spiral}} t) + 2\pi f_{\text{spiral}}\gamma t\cos(2\pi f_{\text{spiral}} t)$.	$v_{\max} = v(t)\vert_{t=T_{\text{end}}}$
Lissajous	$v(t) = \sqrt{\left(x_{\text{size}} - x_{\text{res}}\right)^2 \pi^2 \left(f_x^2 \sin\left(2\pi f_x t\right)^2 + f_y^2 \sin\left(2\pi f_y t\right)^2\right)}$	$v_{\max} = \sqrt{\left(x_{\text{size}} - x_{\text{res}}\right)^2 \pi^2 \left(f_x^2 + f_y^2\right)}$

VI. VERTICAL FEEDBACK BANDWIDTH

The closed-loop bandwidth of the vertical feedback system is a key specification in high-speed microscopy since the topography signal $h(t)$ is effectively low-pass filtered by the complementary sensitivity function. If the topography signal contains frequency content above the closed-loop bandwidth, this information will be lost, introducing imaging artifacts. A varying magnitude and phase response in the frequency range of interest will also introduce imaging artifacts, however this may be compensated by post processing. Constant-height imaging does not require a high bandwidth vertical feedback loop. In this group of imaging modes, the contact force is regulated only by the probe and sample stiffness. Although this results in significantly higher contact forces, the vertical detection bandwidth is limited only by the probe and instrumentation dynamics.

In the remainder of this section, the topography signal bandwidth is derived as a function of the scanning trajectory. During this exercise, the following sinusoidal sample profile is considered

$$h(x, y) = \sin(2\pi f_{\text{profile}} x) + \cos(2\pi f_{\text{profile}} y), \tag{11}$$

where f_{profile} is the number of sample features per micrometer. It may be more convenient to consider the profile period, which is $T_{\text{profile}} = 1/f_{\text{profile}}$, measured in micrometers per feature. The topography and a 3D image of the profile is plotted in Fig. 8. Scanning this profile at a constant velocity v will result in a sinusoidal topography signal, for example, when $y = 0$ and $x = vt$

$$h(t) = \sin(2\pi f_{\text{profile}} vt) + 1. \tag{12}$$

In other words, the frequency is $f_{\text{profile}} \times v$, or v/T_{profile}. In the following, the maximum frequency and spectrum of $h(t)$ is derived for each of the scanning methods, this process reveals the extent to which each method 'spreads' or modulates the frequency content of the sample.

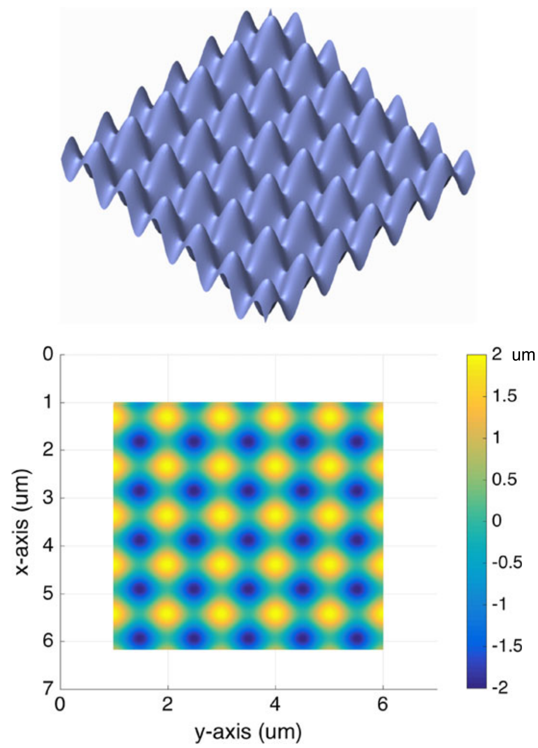

Fig. 8. 2D and 3D view of a sample grating. [Color figure can be viewed at wileyonlinelibrary.com]

6.1 Topography signal frequency

For raster scanning, the frequency of the topography signal was derived in Equation (12) to be $f_{\text{profile}} \times v$. For a sinusoidal raster scan, Equation (11) is approximated as

$$h(x, y) \approx \sin(2\pi f_{\text{profile}} x), \quad x(t) = \sin(2\pi f_{\sin} t),$$

which results in

$$h(t) = \sin\left(2\pi f_{\text{profile}} \sin(2\pi f_{\sin} t)\right). \tag{13}$$

This expression can be simplified by using the Jacobi-Anger identity [42], which is

$$\sin(p\sin(q)) = 2\sum_{n=1}^{\infty} J_{2n-1}(p)\sin([2n-1]q),$$

where $J_{2n-1}(p)$ is the Bessel function of the first kind,

$$J_{\alpha}(p) = \sum_{m=0}^{\infty} \frac{(-1)^m}{m!\Gamma(m+\alpha+1)}\left(\frac{n}{2}\right)^{2m+\alpha},$$

where $\Gamma(.)$ is the gamma function, a shifted generalization of the factorial function to non-integer values. The function (13) can be written as

$$h(t) = 2\sum_{n=1}^{\infty} J_{2n-1}(2\pi f_{\text{profile}})\sin\left[(2n-1)2\pi f_{\sin} t\right],$$

The spectrum contains components at odd multiples of $f_{\sin}$, i.e. $f_{\sin}$, $3f_{\sin}$, $5f_{\sin}$. In addition, the magnitude at each frequency component is scaled by a Bessel function with a value influence by f_{profile}. Despite the complexity, the bandwidth of the spectrum can be estimated by considering the major frequency components that contribute to the total energy of the spectrum. This assumption is similar to Carson's rule which is used in frequency modulation (FM) [43]. Alternatively, the maximum topography disturbance signal bandwidth can be approximated by the maximum velocity and the period of the sample,

$$f_h^{\max} \approx v_{\max} \times f_{\text{profile}} \text{ Hz},$$

where the expression for $v_{\max}$ is described in Section V.

For spiral scans, recall that the trajectories in x and y are

$$x(t) = r(t)\cos(2\pi f_{\text{spiral}} t) \quad y(t) = r(t)\sin(2\pi f_{\text{spiral}} t).$$

The topography signal is found by substituting the trajectories into (11),

$$h(t) = \sin\left(2\pi f_{\text{profile}} r(t)\cos(2\pi f_{\text{spiral}} t)\right) + \cos\left(2\pi f_{\text{profile}} r(t)\sin(2\pi f_{\text{spiral}} t)\right). \tag{14}$$

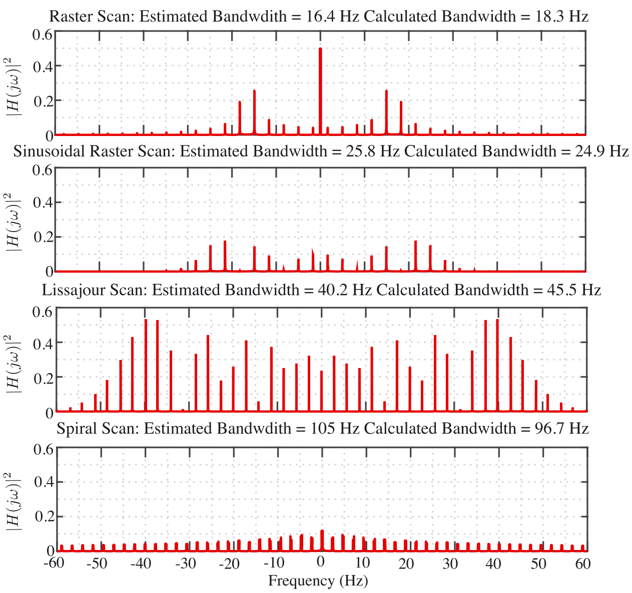

Fig. 9. The frequency spectrum of the topography signal $h(t)$. [Color figure can be viewed at wileyonlinelibrary.com]

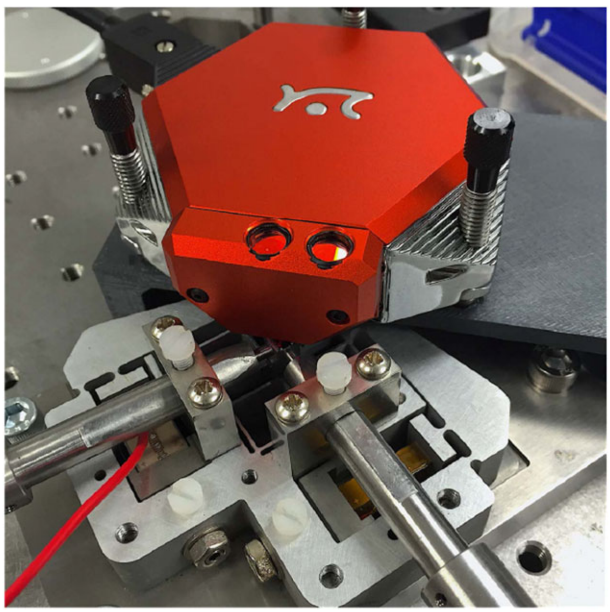

Fig. 10. Experimental set-up. [Color figure can be viewed at wileyonlinelibrary.com]

Table V. A comparison of the analytical and approximated topographic signal bandwidth.

Scan Method	Estimated Bandwidth	Calculated Bandwidth
Raster	16 Hz	18 Hz
Sinusoidal Raster	26 Hz	25 Hz
Lissajous	40 Hz	45 Hz
Spiral	105 Hz	97 Hz

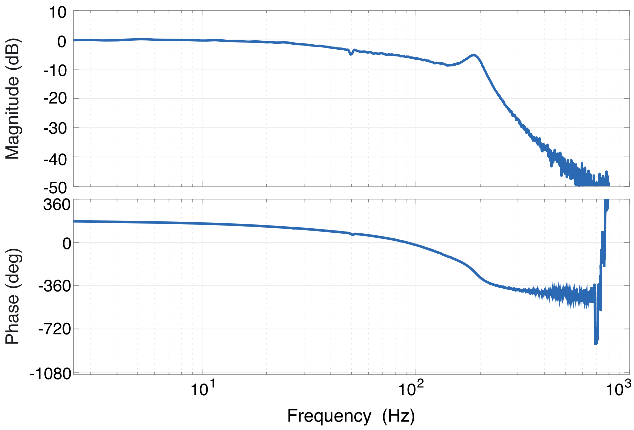

Fig. 11. Measured closed-loop frequency response of the vertical stage in the Nanosurf positioner. The measurement was performed while maintaining constant contact force between the probe tip and sample grating. [Color figure can be viewed at wileyonlinelibrary.com]

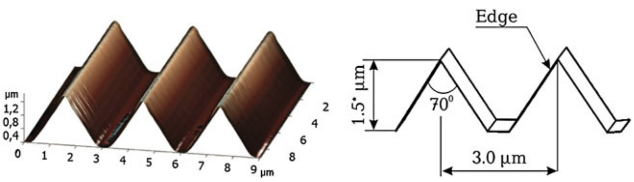

Fig. 12. An NT-MDT TGG1 calibration grating. The grating has a triangular step profile with a height of 1.5 μm and a period of 3.0 μm. [Color figure can be viewed at wileyonlinelibrary.com]

Due to the complexity of this expression, an analytical solution is not given. Instead, the frequency spectrum can be found numerically.

For Lissajous scans, the assumptions for the y-axis in raster and sinusoidal raster scans cannot be applied due to nature of the scanning pattern. Recall that the trajectories are

$$x(t) = A_x \cos(2\pi f_x t), \qquad y(t) = A_y \cos(2\pi f_y t).$$

The topography signal is found by substituting the trajectories into (11),

$$h(t) = \sin\left(2\pi f_{\text{profile}} A_x \cos(2\pi f_x t)\right) + \cos\left(2\pi f_{\text{profile}} A_y \cos(2\pi f_y t)\right), \tag{15}$$

which can be simplified using the Jacobi-Anger identities,

$$\sin\left(p\cos(q)\right) = -2\sum_{n=1}^{\infty}(-1)^n J_{2n-1}(p)\cos\left([2n-1]q\right),$$

$$\cos\left(p\cos(q)\right) = J_0(p) + 2\sum_{n=1}^{\infty}(-1)^n J_{2n}(p)\cos\left(2nq\right),$$

hence (15) can be written as

$$h(t) = -2\sum_{n=1}^{\infty}(-1)^n J_{2n-1}(p_1)\cos\left([2n-1]q_1\right) + J_0(p_2) + 2\sum_{n=1}^{\infty}(-1)^n J_{2n}(p_2)\cos\left(2nq_2\right) \tag{16}$$

where $p_1 = 2\pi f_{\text{profile}} A_x$, $q_1 = 2\pi f_x t$, $p_2 = 2\pi f_{\text{profile}} A_x$ and $q_2 = 2\pi f_y t$.

The findings above are illustrated by the example profile shown in Fig. 8. The image size is 5×5μm with a resolution of 50 nm. The imaging time is chosen to be 60 s which results in a scanning frequency of 1.658 Hz for the raster and sinusoidal raster scans. The Lissajous scan rates are $f_x = 1.833$ Hz and $f_y = 1.825$ Hz. The spiral scan rate is 1.172 Hz. The topography signal spectra for each scanning method are plotted in Fig. 9. These plots were created by numerically simulating an entire scan and computing the power spectral density of $h(t)$. The bandwidth of the spiral scan is the broadest, followed by the Lissajous scan due to the high probe velocities. Table V lists the frequency where 95% of the signal is contained below. As predicted analytically, the lowest bandwidth is achieved for raster scanning, followed by sinusoidal raster scanning, Lissajous scanning and spiral scanning. Despite having the lowest scanning frequency, spiral scanning requires a five times greater vertical bandwidth than raster scanning. Due to the significantly increased vertical bandwidth, spiral scanning is not considered in the following experimental examination.

6.2 Experimental results

In this section, the findings in Section 6.1 are validated experimentally. As pictured in Fig. 10, the experimental setup is a high-speed xy flexure-guided nanopositioner and Nanosurf EasyScan 2 AFM. The lateral scanner has a range of 25 μm by 25 μm and a resonance frequency of 2.7 kHz [4]. In the experiment, the x and y axes are controlled using an inverse controller with integral action. A closed-loop bandwidth of 680 Hz was achieved while maintaining a 10 dB gain margin. This bandwidth is sufficient to ensure that lateral positioning errors are negligible.

The vertical stage was implemented using a Nanosurf AFM with a z-axis range of 22 μm. The AFM images presented here are obtained in constant-force contact-mode. The PID controller was tuned to the manufacturer's recommended values. The measured closed-loop frequency response of the vertical stage is shown in Fig. 11, which reveals a bandwidth of 45 Hz.

An NT-MDT TGG1 calibration grating is used to evaluate the images, see Fig. 12. The grating has a triangular profile with a height of 1.5 μm and a period of 3.0 μm. The topographies and 3D images of the sample were constructed by plotting the control signal $u(t)$ to the z-axis actuator versus the x and y position of the sample.

The topography, profile and 3D image of an 18 μm scan is plotted in Fig. 13. The reference image was recorded with a scan rate of 0.2 Hz to avoid any bandwidth related artefacts. The experimental results compare the quality of an 18μm scan with 128 pixels per line. The two imaging times were 128 s and 256 s with a sampling frequency of 400 Hz.

In Case 1, the imaging time is 256 s which requires a 0.5-Hz scan rate for the raster and sinusoidal raster methods. The Lissajous scan rates were f_x = 0.5586 Hz and f_y = 0.5566 Hz. The simulated and experimental topography spectra are plotted in Fig. 14a. The simulation was based on a triangular wave profile with a height of 1.5 μm and a period of 3 μm. It can be observed that a higher topography bandwidth is required for the sinusoidal raster and Lissajous scanning methods.

In Case 2, the imaging time is 128 s which requires a 1-Hz scan rate for the raster and sinusoidal raster methods. The Lissajous scan rates were f_x = 1.1172 Hz and f_y = 1.1133 Hz. The simulated and experimental topography spectra are plotted in Fig. 14b. These results show an identical trend to case 1; however, with the higher scan rates, an obvious smoothing artefact can be observed in the high velocity regions of the sinusoidal and Lissajous methods.

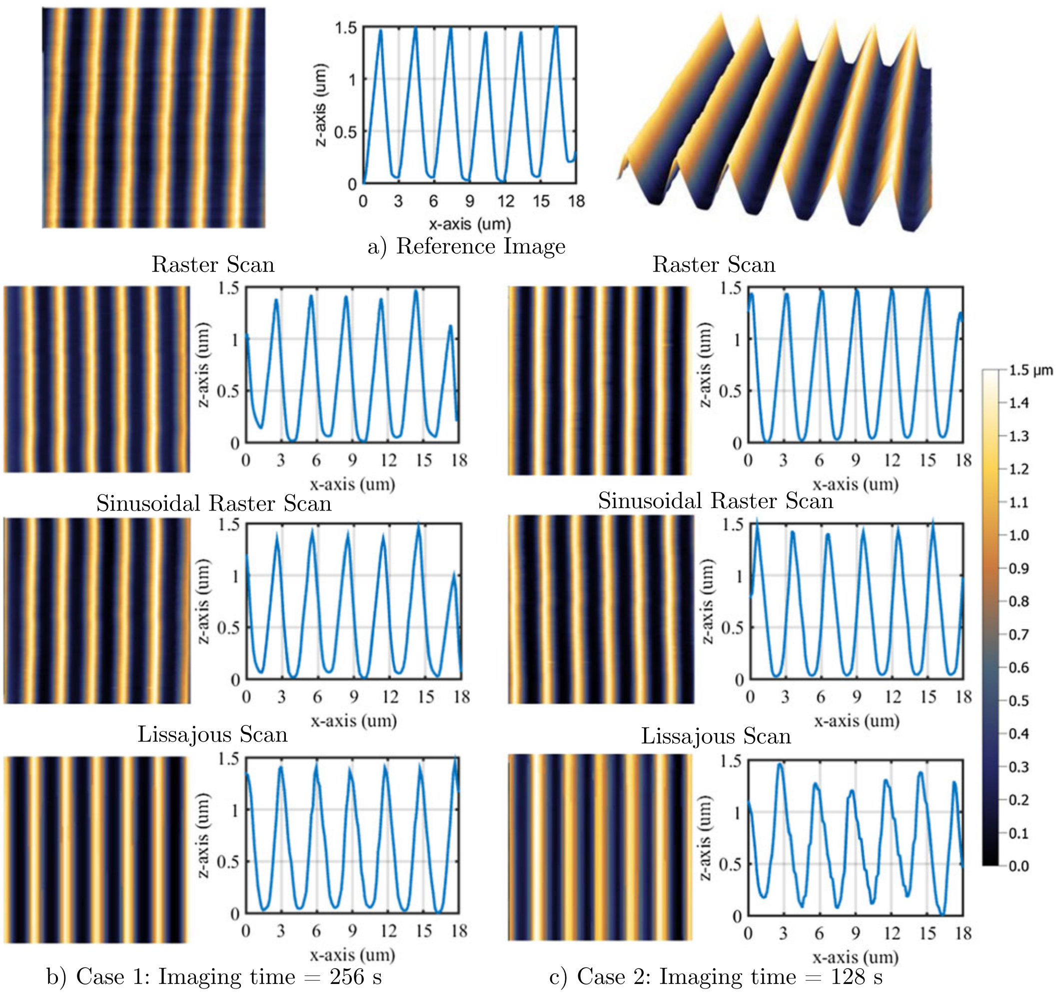

Fig. 13. (a) A reference image of the TGG1 calibration grating. (b) The profiles and topographies for raster, sinusoidal raster and Lissajous scans for a fixed imaging time of 256 s. (c) The profiles and topographies for raster, sinusoidal raster and Lissajous scans for a fixed imaging time of 128 s . [Color figure can be viewed at wileyonlinelibrary.com]

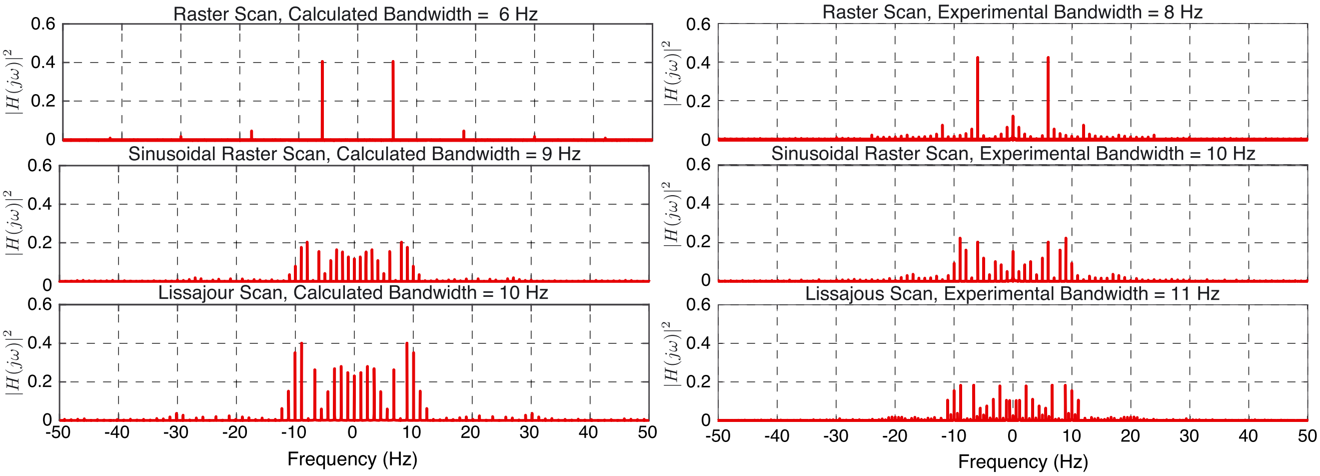

(a) Case 1: The frequency spectrum in the topographic signal for each scanning methods with an imaging time of 256 s. Simulation results (left), experimental results (right).

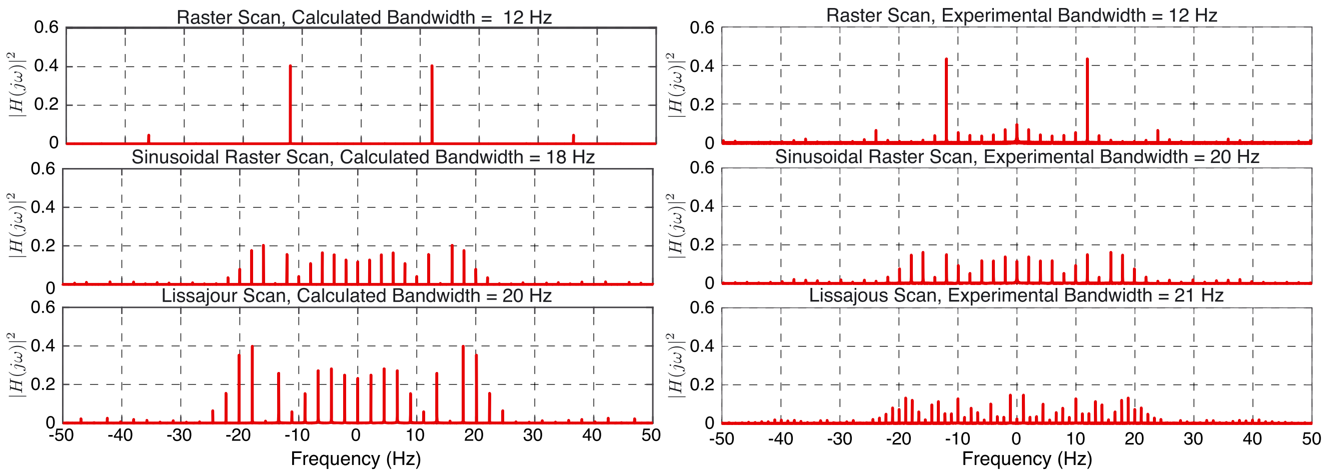

(b) Case 2: The frequency spectrum in the topographic signal for different scanning methods with an imaging time of 128 s. Simulation results (left), experimental results (right).

Fig. 14. A comparison of frequency spectrums for the topographical signals in each scanning methods. In case 1, the imaging time is fixed as 256 s and in case 2 the imaging time is fixed as 128 s. [Color figure can be viewed at wileyonlinelibrary.com]

VII. CONCLUSION

This article investigates the performance and control consequences of novel SPM scanning trajectories such as sinusoidal raster scanning, spiral scanning, and Lissajous scanning. These methods can significantly increase the maximum scan rate but at the expense of varying probe velocity and increased vertical bandwidth.

Of the sinusoidal methods, the spiral method is found to require the lowest scanning frequency and the sinusoidal raster method is found to have the lowest probe velocity for a given imaging time and resolution.

The lateral scanning trajectory also influences the bandwidth and spectrum of the topography signal used to construct the image. Since the vertical feedback system is often severely limited in bandwidth, it is desirable to minimize the topography signal bandwidth. Although the novel scanning methods improve the lateral performance, they also significantly increase the probe velocity and consequently, the bandwidth of the topography signal compared to traditional raster scanning.

Experimental imaging demonstrated a smoothing artefact associated with Lissajous scanning due to the higher probe velocity and topography bandwidth.

Therefore, a trade-off exists between the lateral and vertical performance. The conclusion of this investigation is that traditional raster scanning or a variant should be used if the scanning frequency is well within the bandwidth of the lateral scanner. In high-speed applications where a sinusoidal method is required, the sinusoidal raster method will require the lowest sampling frequency, probe velocity, and topography bandwidth compared to the other methods considered.

REFERENCES

1. Salapaka, S. M. and M. V. Salapaka, "Scanning probe microscopy," *IEEE Control Syst. Mag.*, Vol. 28, No. 2, pp. 65–83 (2008).
2. Binnig, G., H. Rohrer, C. Gerber, and E. Weibel, "Surface studies by scanning tunnelling microscopy," *Phys. Rev. Lett.*, Vol. 49, No. 1, pp. 57–61 (1982).
3. Binnig, G., C. F. Quate, and C. Gerber, "Atomic force microscope," *Phys. Rev. Lett.*, Vol. 56, No. 9, pp. 930–933 (1986).
4. Yong, Y. K., S. S. Aphale, and S. O. R. Moheimani, "Design, identification, and control of a flexure-based XY stage for fast nanoscale positioning," *IEEE Trans. Nanotechnol.*, Vol. 8, No. 1, pp. 46–54 (2009).
5. Clayton, G. M., S. Tien, and K. K. Leang, "A review of feedforward control approaches in nanopositioning for high-speed SPM," *J. Dyn. Syst. Meas. Control-Trans. ASME*, Vol. 131, No. 6, pp. 061101-1–061101-19. (2009).
6. Schitter, G., K. J. Astrom, B. E. DeMartini, P. J. Thurner, K. L. Turner, and P. K. Hansma, "Design and modelling of a high-speed AFM scanner," *IEEE Trans. Control Syst. Technol*, Vol. 15, No. 5, pp. 906–915 (2007).
7. Devasia, S., E. Eleftheriou, and S. O. R. Moheimani, "A survey of control issues in nanopositioning," *IEEE Trans. Control Syst. Technol*, Vol. 15, No. 5, pp. 802–823 (2007).
8. Ando, T., "Control techniques in high-speed atomic force microscopy," *Proc. Amer. Control Conf.*, Seattle, Washington, pp. 3194–3200 (2008).
9. Butterworth, J. A. and L. Y. Pao, "A comparison of control architectures for atomic force microscopes," *Asian J. Control*, Vol. 11, No. 2, pp. 175–181 (2009).
10. Chuang, N., I. R. Petersen, and H. R. Pota, "Robust H(infinity) control in fast atomic force microscopy," *Asian J. Control*, Vol. 15, No. 3, pp. 872–887 (2013).
11. Fleming, A. J. and A. G. Wills, "Optimal periodic trajectories for band-limited systems," *IEEE Trans. Control Syst. Technol.*, Vol. 17, No. 3, pp. 552–562 (2009).
12. Vaughan, J., A. Yano, and W. Singhose, "Robust negative input shapers for vibration suppression," *J. Dyn. Syst. Meas. Control-Trans. ASME*, Vol. 131, No. 3, pp. 031014-1–031014-9 (2009).
13. Croft, D., G. Shed, and S. Devasia, "Creep, hysteresis, and vibration compensation for piezoactuators: Atomic force microscopy application," *J. Dyn. Syst. Meas. Control-Trans. ASME*, Vol. 123, No. 1, pp. 35–43 (2001).
14. Clayton, G. M. and S. Devasia, "Image-based compensation of dynamic effects in scanning tunnelling microscopes," *Nanotechnology*, Vol. 16, No. 6, pp. 809–818 (2005).
15. Fleming, A. J., B. J. Kenton, and K. K. Leang, "Bridging the gap between conventional and video-speed scanning probe microscopes," *Ultramicroscopy*, Vol. 110, No. 9, pp. 1205–1214 (2010).
16. Chen, C. L., J. W. Wu, Y. T. Lin, Y. T. Lo, and L. C. Fu, "Sinusoidal trajectory for atomic force microscopy precision local scanning with auxiliary optical microscopy," *Proc. 52nd IEEE Conf. Decis. Control*, Florence, Italy, pp. 348–353 (2013).
17. Leang, K. K., "Iterative learning control of hysteresis in piezo-based nanopositioners," *Ph.D. thesis*, University of Washington, Seattle, WA (2004).
18. Leang, K. K. and S. Devasia, "Feedback-linearised inverse feed-forward for creep, hysteresis, and vibration compensation in AFM piezoactuators," *IEEE Trans. Control Syst. Technol*, Vol. 15, No. 5, pp. 927–935 (2007).
19. Mahmood, I. A. and S. O. R. Moheimani, "Fast spiral-scan atomic force microscopy," *Nanotechnology*, Vol. 20, No. 36, pp. 1–4 (2009).
20. Kotsopoulos, A. G. and T. A. Antonakopoulos, "Nanopositioning using the spiral of Archimedes: The probe-based storage case," *Mechatronics*, Vol. 20, No. 2, pp. 273–280 (2010).
21. Hung, S. K., "Spiral scanning method for Atomic Force Microscopy," *J. Nanosci. Nanotechnol.*, Vol. 10, No. 7, pp. 4511–4516 (2010).
22. Mahmood, I. A., S. O. R. Moheimani, and B. Bhikkaji, "A new scanning method for fast Atomic Force Microscopy," *IEEE Trans. Nanotechnol.*, Vol. 10, No. 2, pp. 203–216 (2011).
23. Rana, M. S., H. R. Pota, I. R. Petersen, and H. Habibullah, "Spiral scanning of atomic force microscope for faster imaging," *Proc. 52nd IEEE Conf. Decis. Control*, Florence, Italy, pp. 354–359 (2013).
24. Bazaei, A., Y. K. Yong, and S. O. R. Moheimani, "High-speed Lissajous-scan atomic force microscopy: Scan pattern planning and control design issues," *Rev. Sci. Instrum.*, Vol. 83, No. 6, pp. 063701–10 (2012).
25. Tuma, T., J. Lygeros, V. Kartik, A. Sebastian, and A. Pantazi, "High-speed multiresolution scanning

probe microscopy based on Lissajous scan trajectories," *Nanotechnology*, Vol. 23, No. 18, pp. 185501–10 (2012).
26. Yong, Y. K., A. Bazaei, and S. O. R. Moheimani, "Video-rate Lissajous-scan atomic application to Atomic Force Microscopy," *Proc. Amer. Control Conf.*, pp. 3516–3521 (2007).
27. Yong, Y. K., S. O. R. Moheimani, and I. R. Petersen, "High-speed cycloid-scan atomic force microscopy," *Nanotechnology*, Vol. 21, No. 36, pp. 365503–5 (2010).
28. De Berg, M., M. Van Kreveld, M. Overmars, and O. C Schwarzkopf, *Computational Geometry*, Springer (2000).
29. Andersson, S. B. and D. Y. Abramovitch, "A survey of non-raster scan methods with application to Atomic Force Microscopy," *Proc. Amer. Control Conf.*, New York, pp. 3516–3521 (2007).
30. Garca, R. and R. Perez, "Dynamic atomic force microscopy methods," *Surf. Sci. Rep.*, Vol. 47, No. 6–8, pp. 197–301 (2002).
31. Fleming, A. J., "Dual-stage vertical feedback for high-speed Scanning Probe Microscopy," *IEEE Trans. Control Syst. Technol.*, Vol. 19, No. 1, pp. 156–165 (2011).
32. Leang, K. K. and A. J. Fleming, "High-speed serial-kinematic SPM scanner: design and drive considerations," *Asian J. Control*, Vol. 11, No. 2, pp. 144–153 (2009).
33. Hara, S., Y. Yamamoto, T. Omata, and M. Nakano, "Repetitive control system: a new type servo system for periodic exogenous signals," *IEEE Trans. Autom. Control.*, Vol. 33, No. 7, pp. 659–668 (1988).
34. Necipoglu, S., S. A. Cebeci, Y. E. Has, L. Guvenc, and C. Basdogan, "Robust repetitive controller for fast AFM imaging," *IEEE Trans. Nanotechnol.*, Vol. 10, No. 5, pp. 1074–1082 (2012).
35. Teo, Y. R., A. A. Eielsen, J. T. Gravdahl, and A. J. Fleming, "Discrete-time repetitive control with model-less FIR filter inversion for high performance nanopositioning," *Proc. IEEE/ASME Adv. Intell. Mechatron.*, Besancon, France, pp. 1664–1669 (2014).
36. Teo, Y. R. and A. J. Fleming, "A new repetitive control scheme based on non-causal FIR filters," *Proc. Amer. Control Conf.*, pp. 991–996 (2014).
37. Kenton, B. J. and K. K. Leang, "Design and control of a three-axis serial-kinematic high-bandwidth nanopositioner," *IEEE/ASME Trans. Mechatron.*, Vol. 17, No. 2, pp. 356–369 (2012).
38. Teo, Y. R., A. J. Fleming, A. A. Eielsen, and J. T. Gravdahl, "A simplified method for discrete-time repetitive control using model-less Finite Impulse Response filter inversion," *J. Dyn. Syst. Meas. Control-Trans. ASME*, Vol. 138, No. 8, pp. 081002-1–081002-13 (2016).
39. Habibullah, H., I. R. Petersen, H. R. Pota, and M. S. Rana, "LQG controller with sinusoidal reference signal modeling for spiral scanning of atomic force microscope," *Proc. Int. Conf. Ind. Electron. Applicat.*, Seattle, Washington, pp. 1474–1479 (2013).
40. Habibullah, H., H. R. Pota, and I. R. Petersen, "High-precision spiral positioning control of a piezoelectric tube scanner used in an atomic force microscope," *Proc. Amer. Control Conf.*, Portland, Oregon, pp. 1625–1630 (2014).
41. Bazaei, A., A. G. Fowler, M. Maroufi, and S. O. Reza Moheimani, "Tracking of spiral trajectories beyond scanner resonance frequency by a MEMS nanopositioner," *2015 IEEE Conference on Control Applications (CCA)*, Sydney, Australia, pp. 1014–1019 (September 21–23, 2015).
42. Abramowitz, M. and I. A. Stegun, *Handbook of mathematical functions. with formulas, graphs, and mathematical tables*, Courier Corporation (2012).
43. Carson, J. R., "Notes on the theory of modulation," *Proc. Inst. Radio Engineers*, Vol. 10, No. 1, pp. 57–64 (1922).

Yik R. Teo graduated from The University of Newcastle, Australia (Callaghan campus) with a Bachelor of Electrical Engineering (1st Class Honors) in 2010 and a Master of Philosophy in Mechanical Engineering in 2013. He is currently pursuing his Ph.D. under the supervision of Dr. Andrew J Fleming at the Precision Mechatronics Lab located at The University of Newcastle, Australia. His research includes high-precision positioning, scanning probe microscopy, and nano-fabrication. Academic awards include the Glenn and Ken Moss Research Higher Degree Award, Australian Postgraduate Award and the Vice-Chancellor Award in Outstanding Research Candidate.

Andrew J. Fleming graduated from The University of Newcastle, Australia (Callaghan campus) with a Bachelor of Electrical Engineering in 2000 and Ph.D in 2004. Dr. Fleming is presently an Australian Research Council Future Fellow and Director of the Precision Mechatronics Lab at The University of Newcastle, Australia. His research interests include biomedical devices, lithography, nano-positioning, and scanning probe microscopy. Dr. Fleming's research

awards include the IEEE Transactions on Control Systems Technology Outstanding Paper Award and The University of Newcastle Researcher of the Year Award. He is the co-author of three books and more than 170 Journal and Conference articles. Dr. Fleming is the inventor of several patent applications, and in 2012 he received the Newcastle Innovation Rising Star Award for Excellence in Industrial Engagement.

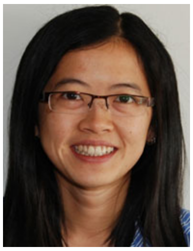

Yuen Kuan Yong received the B.Eng. degree (1st Class Hons.) in mechatronic engineering and the Ph.D. degree in mechanical engineering from The University of Adelaide, Australia, in 2001 and 2007, respectively. She is currently an Australian Research Council DECRA Fellow with the School of Electrical Engineering and Computer Science, The University of Newcastle, Australia. Her research interests include the design and control of nanopositioning systems, high-speed atomic force microscopy, finite-element analysis of smart materials and structures, sensing and actuation, and design and control of miniature robots. Dr. Yong is a recipient of the 2016 and 2008 IEEE/ASME International Conference on Advanced Intelligent Mechatronics (AIM) Best Conference Paper Finalist Award, The University of Newcastle Vice-Chancellor's Awards for Research Excellence and the Pro Vice-Chancellor's Award for Excellence in Research Performance. She is an Associate Editor for Frontiers in Mechanical Engineering (specialty section Mechatronics) and the International Journal of Advanced Robotic Systems. She is also a steering committee member for the 2016 International Conference on Manipulation, Automation and Robotics at Small Scales (MARSS).